ACS Photonics

pubs.acs.org/journal/apchd5

Letter

Large-Scale Inverse Design of a Planar On-Chip Mode Sorter

Giuseppe Di Domenico,*[,§] Dror Weisman,[§] Annibale Panichella, Dolev Roitman, and Ady Arie

Cite This: *ACS Photonics* 2022, 9, 378−382

Read Online

ACCESS | Metrics & More | Article Recommendations

ABSTRACT: Spatial modes of light can be used as carriers of information in classical optical communication or as an alphabet in quantum optical communication. In order to exploit the spatial domain, it is required to (de)multiplex different modes from a shared input channel into different output ports. Mode sorters have been employed in free-space and fiber systems but to date have not been realized for planar guided waves. Here we present a general method for compact on-chip sorting of different planar beams with a micrometric footprint and nanometric thickness. The designs were generated using a linkage-tree-based genetic algorithm and were experimentally demonstrated on a surface plasmon polariton platform by sorting of Hermite−Gaussian beams. The method used here can be readily applied to optimize complex, large-scale optical devices involving beam propagation methods.

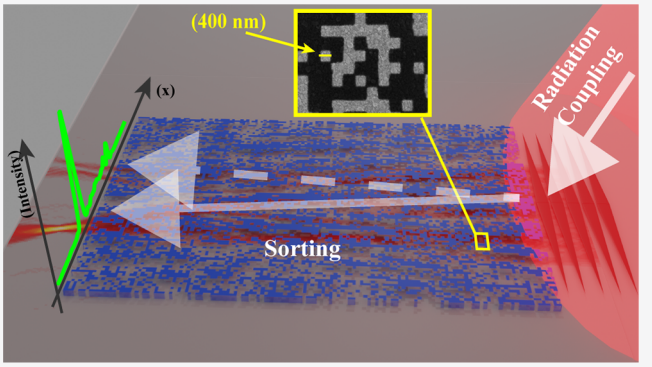

KEYWORDS: *integrated photonics, mode (de)multiplexing, dielectric metasurface, genetic algorithm optimization, subwavelength grating*

Downloaded via NANJING UNIV on February 18, 2022 at 14:33:29 (UTC).
See https://pubs.acs.org/sharingguidelines for options on how to legitimately share published articles.

The spatial degree of freedom of light beams is attractive both in classical communications and in quantum communications, since it is relatively resilient to noise and unbounded in dimensionality.[1] A set of orthogonal spatial modes, based for example on either Laguerre−Gaussian or Hermite−Gaussian (HG) modes, can be used as carriers of information to increase the capacity of classical communications systems by space division multiplexing[2−4] or as an alphabet for secure quantum communication applications.[5,6] These systems rely on the ability to sort the different beams at the input and output ports. Beam sorting has been developed for free-space systems,[7−9] waveguide-integrated configurations,[10−13] and fiber communication systems,[14] but the requirement to process and transmit signals at the chip level necessitates extending these sorting capabilities to planar integrated optical devices.[15] To date this problem has been addressed only for routing of free-space vortex beams on a chip.[16]

Here we propose a compact solution, embedded on a chip, for sorting and coupling of planar beams with different spatial wavefronts. Specifically, we experimentally demonstrate demultiplexer devices for HG plasmonic beams. Surface plasmon polaritons (SPPs) are electromagnetic waves that propagate at the interface between a metal and a dielectric and are excellent candidates to bridge the gap between optical and electrical signals.[17,18] When subwavelength dielectric pixels with nanometric thickness are placed on top of a metal−air interface, a small change in the effective refractive index can be achieved at specific positions along the propagation of the SPPs, since these are highly confined to the interface. This property allows us to design and control the propagation of different spatial modes in a flexible manner. The result is a single-element on-chip device with a micrometric footprint and nanometric thickness that can be integrated into an array and easily coupled to other photonic/plasmonic circuits.

We have designed and fabricated two sorters, one for sorting two HG beams and the other for sorting three HG beams. The two-beam sorter was manufactured on a silver layer; a scheme of the setup is shown in Figure 1a. A 70 nm silver layer was evaporated on a BK7 glass substrate and then spin-coated with a poly(methyl methacrylate) (PMMA) resist at 4000 rpm to achieve a thickness of 50 nm. Electron lithography was used to make the desired pattern of the device, followed by focused ion beam (FIB) milling within the silver layer to add a grating coupler. To excite the desired HG plasmonic beam at the silver−air interface, an input-modulated grating coupler[19,20] is illuminated with a 1.064 μm laser. We note that the sorting capabilities are independent of the excitation method, and similar sorting performance is expected for other methods of generating the beams, such as selective excitation[21] and end-fire coupling.[22] The plasmon beam then propagates through

Received: October 9, 2021
Published: January 24, 2022

ACS Publications

© 2022 The Authors. Published by American Chemical Society

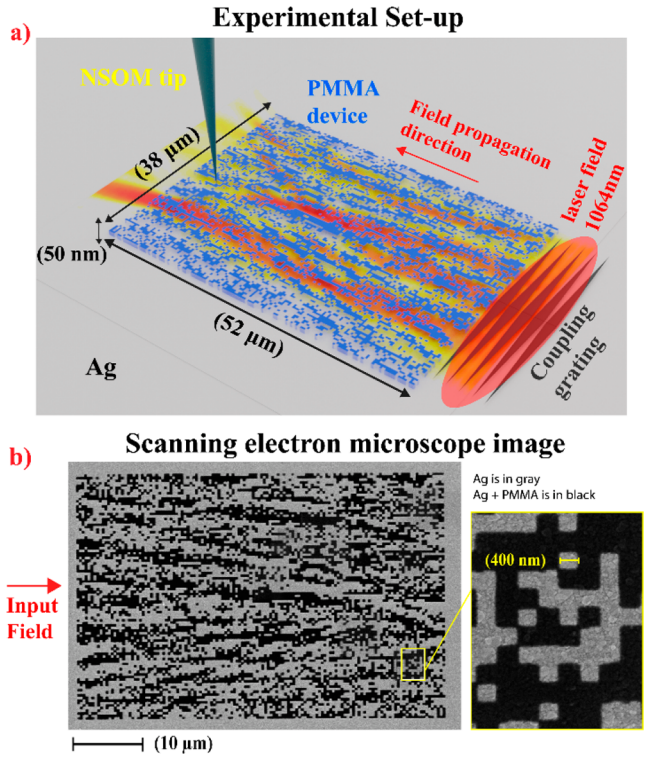

Figure 1. (a) Scheme of the experimental setup. Different HG plasmonic modes are excited from free space using a grating coupler, and the sorter routs each beam into a selected output port. (b) Scanning electron microscope image of the two-beam demultiplexer device.

the device, and the plasmon near-field intensity distribution is collected using a Nanonics MultiView 2000 NSOM system. The two-beam sorter device is contained in a 52 μm × 38 μm region. The distribution of a thin layer (50 nm) of PMMA results in an effective refractive index difference (Δn) of ~0.040. The result is shown in Figure 1b, where the silver sections are shown in bright gray and the silver + PMMA sections are dark.

The optimization uses a genetic algorithm called the linkage learning nondominated sorting genetic algorithm (L2-NSGA)[23,24] to generate and optimize the devices iteratively. The pseudocode is presented in Figure 2a. The algorithm starts by initializing a pool (or population) of M = 1000 device realizations (called individuals), as shown in step I in Figure 2a. These devices are randomly generated using pseudorandom number generation (line 2). Each device in the pool is encoded as a 95 × 130 binary matrix for the two-beam sorter. Each matrix element corresponds to the presence or absence of the PMMA layer in a 400 nm × 400 nm region at a set location. Each generated device is then evaluated using the beam propagation method (BPM). Next, the pool is evolved within the main loop in lines 3−20. In each iteration, new devices are created by selecting two devices in the population, one parent (line 7) and one donor (line 8), using tournament selection. This routine provides more selection chances to the devices with output fields closer to the specified target fields. Then a new device (called the offspring) is generated in lines 9 and 10 using L2-CROSSOVER and MUTATION by combining the genes (pixels) in the parent and donor devices. In the example shown in Figure 2a, the offspring is generated by cloning the parent device and replacing certain pixels (indexes from 11 to 16) with the values extracted from the donor. The indexes of the gene/pixel to extract are determined using a machine learning (ML) model that is trained at the beginning of each iteration (line 4). L2-NSGA uses agglomerative hierarchical clustering (AHC), which returns the family of subsets (FOS) (see the dendrogram in Figure 2a), corresponding to the groups of genes (nodes in the dendrogram) that should not be broken up according to the AHC algorithm. Besides, each child is further mutated using bit-flip mutation, which randomly bit-flips the pixels in the target device (line 10). Finally, the best 1000 devices among parents and offspring are selected to form the population for the next generation (lines 12−20). The code we used has been made available.[25] The plot in Figure 2b shows the fitness value at every iteration (generation) in the optimization process in the case of the two-beam sorter. For the fitness value, we consider the norm of the difference between the output field from the device (evaluated with the BPM) and the target specified field. The insets show how the device evolves at different stages to improve its fitness value. We note that the successful implementation of L2-NSGA shown here highlights the broad applicability of this method in optics, as it can be used to optimize a wide range of complex optical devices that

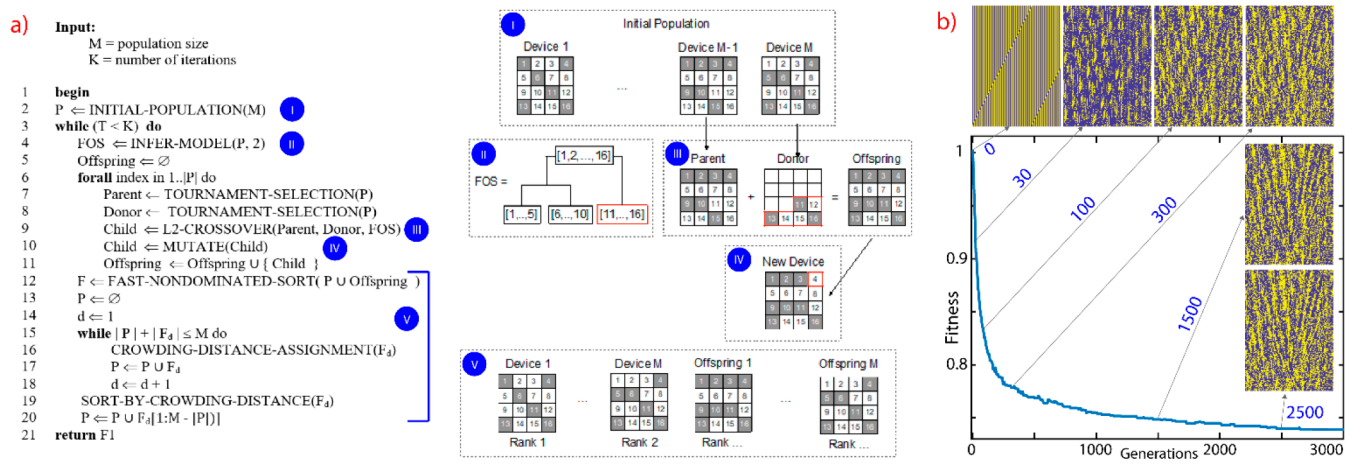

Figure 2. (a) Pseudocode of the algorithm and graphical representation of the different steps. (b) Plot of the fitness values as generations progress. The insets show the best devices found by the algorithm in the selected generations.

https://doi.org/10.1021/acsphotonics.1c01539
ACS Photonics 2022, 9, 378−382

involve beam propagation techniques. In particular, with regard to embedded applications, this algorithm easily handles components with wide footprints or arrays of multiple components. The algorithm is specifically suited for problems where a large number of variables must be optimized together in order to find a global solution.

In the case shown here, as the target function we choose to focus energy at the end of the device onto two separate spots depending on whether the input plasmonic beam is a zeroth-order (HG0) or first-order (HG1) Hermite−Gaussian beam. In Figure 3a1, we use the BPM to simulate the propagation

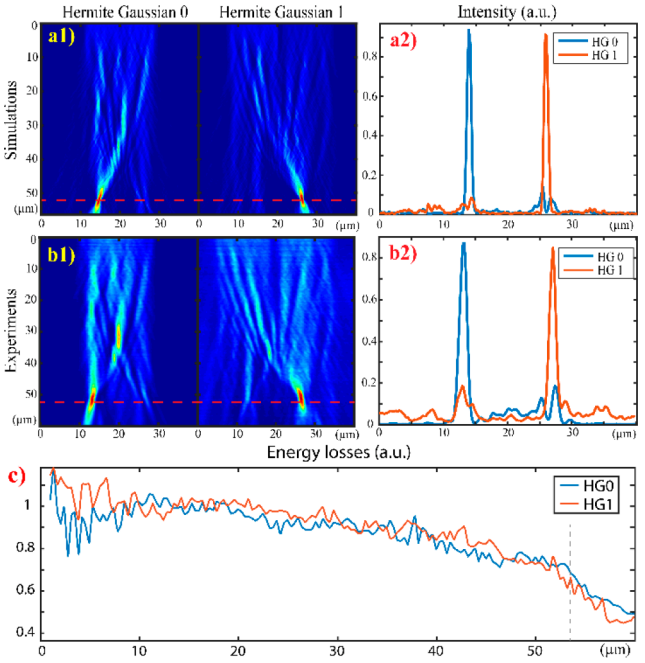

Figure 3. (a1) Numerical simulations and (b1) experimental measurements of the SPP intensity distribution along the two-beam demultiplexer for HG0 and HG1 inputs. The red dashed line indicates where the device ends. (a2) Simulated and (b2) measured intensity profiles at the end of the device for the two inputs. The experimental data were measured with the same sorter but with different grating couplers. (c) Plot of the measured energy vs the propagation inside the two-beam device. The gray dashed line indicates where the device ends.

through the sorter of HG0 on the left and HG1 on the right. As can be seen, the demultiplexer routes the two different beams into the two desired spots. Figure 3a2 shows the intensity at the end of the device, represented by the red cross-section dashed line in Figure 3a1. The crosstalk between the two channels is smaller than 0.12. Figure 3b1 and Figure 3b2 are the analogues of Figure 3a1,a2 with experimental data. It is clearly seen that the system behaves as predicted, as the spot sizes, positions, and intensities are in excellent agreement with the simulations. We have also realized a 72 μm × 36 μm three-mode demultiplexer that sorts HG0, HG1, and HG2 plasmonic beams. Figure 4 reports the (a) numerical and (b) experimental results, which show how the different inputs are focused on spatially separate spots. Figure 4c presents a comparison of the intensity distributions at the end of the device for the different input modes.

The propagation losses of the device were measured from the experiments, and Figure 3c displays the power (the

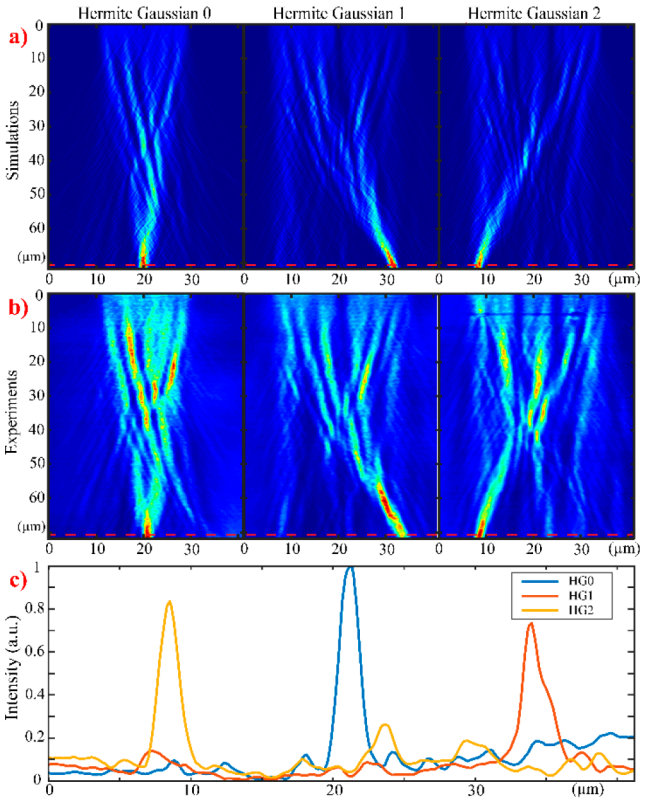

Figure 4. (a) Numerical and (b) near-field-measured SPP intensity distributions for a three-beam demultiplexer for (left to right) zeroth-, first-, and second-order HG beams. (c) Comparison of the intensity distributions at the end of the device originated from different inputs.

intensity measured by the NSOM integrated along the transverse direction) as it propagates inside the device. In the experimental data, as the initial power we use the value at 8 μm from the device input; before that point, the measurement is affected by scattering from the grating. The final power is integrated on the device output 52 μm from the start. The power transmission for the two-mode sorter is 74% for HG0 and 67% for HG1, compared with a theoretical transmission of 96.7% for 44 μm propagation on a flat surface without the mode sorter. The losses of the flat surface are determined by the silver permittivity. At our wavelength, $\epsilon_{\text{Silver}} = -58.04 + i0.61$.[26] Hence the excess loss due to the sorter is, on average, 26%. If we consider the amount of energy that reaches the target regions, from our measurement we found that the device couples 38% and 27% (for HG0 and HG1, respectively) of the total energy measured at 8 μm from the device input. The spectral bandwidth of our design is dominated by the dispersion of the metal. Although the algorithm does not specifically optimize for large bandwidth, our simulations show that the crosstalk remains below 0.25 in the range between 970 and 1090 nm.

Finally, we tested the robustness of our design by varying the beam input position and angle to simulate misalignments and by varying the effective refractive index value of the dielectric with respect to the nominal value, which can happen in physical systems as a result of variation in the thickness of the pixel. We found that for displacements of the input beams of up to ±2 μm or changes the input angle of up to ±4 mrad, the crosstalk remains below 0.25. The design is relatively robust with respect to variations in Δn as a result of changes in the

https://doi.org/10.1021/acsphotonics.1c01539
ACS Photonics 2022, 9, 378−382

dielectric height. To keep the crosstalk smaller than 0.25, we can reduce Δn by up to 28%. On the contrary, increasing Δn further reduces the crosstalk (we reached 0.16 for a 20% increase). However, using FDTD simulations, we found that a high Δn creates backscattering that ruins the functionality of the device.

In summary, we have shown a new way to design a compact on-chip mode sorter that can be applied for a variety of wave fronts. As a proof of concept, we have designed and fabricated micrometric, single element, solid-state demultiplexers for HG beams. Our algorithm has been used to optimize the refractive index distributions, but the method is general and can be adapted to generate linear or nonlinear complex devices that perform other functions specified by the user. Moreover, our method can optimize large-scale devices in a relatively short time, making this method competitive when multiple optical components need to function together on the same wafer and their functionalities as well as the relative couplings between the components need to be globally optimized. The devices proposed here can be used for spatial sorting of different planar beams when these are coupled to free-space beams or to a photonic/plasmonic chip. Therefore, it enables different input beams to be routed to different devices on the chip. The sorter can be readily integrated with active plasmonic devices such as electronic−plasmonic high-speed transmitters,[27] enabling the generated signals to be routed into multiple devices. Alternatively, an active plasmonic mode converter[28] can be positioned before the demultiplexer to dynamically change the input into the device.

AUTHOR INFORMATION

Corresponding Author

Giuseppe Di Domenico − *School of Electrical Engineering, Fleischman Faculty of Engineering, Tel-Aviv University, Tel Aviv 69978, Israel;* orcid.org/0000-0003-2109-9137; Email: giuseppedidomenico8@gmail.com

Authors

Dror Weisman − *School of Electrical Engineering, Fleischman Faculty of Engineering, Tel-Aviv University, Tel Aviv 69978, Israel*

Annibale Panichella − *Software Technology, Delft University of Technology, 2628 XE Delft, The Netherlands*

Dolev Roitman − *School of Electrical Engineering, Fleischman Faculty of Engineering, Tel-Aviv University, Tel Aviv 69978, Israel;* orcid.org/0000-0002-1111-026X

Ady Arie − *School of Electrical Engineering, Fleischman Faculty of Engineering, Tel-Aviv University, Tel Aviv 69978, Israel;* orcid.org/0000-0001-6486-7285

Complete contact information is available at: https://pubs.acs.org/10.1021/acsphotonics.1c01539

Author Contributions

[§]G.D.D. and D.W. contributed equally.

Notes

The authors declare no competing financial interest.

ACKNOWLEDGMENTS

This work was supported by the Pazy Foundation, the Israel Ministry of Science, Technology and Space, and the Israel Science Foundation (Grant 1415/17).

REFERENCES

(1) Cox, M. A.; Maqondo, L.; Kara, R.; Milione, G.; Cheng, L.; Forbes, A. The resilience of Hermite−and Laguerre−Gaussian modes in turbulence. *J. Light. Technol.* **2019**, *37*, 3911−3917.

(2) Wang, J.; Yang, J. Y.; Fazal, I. M.; Ahmed, N.; Yan, Y.; Huang, H.; Ren, Y.; Yue, Y.; Dolinar, S.; Tur, M.; Willner, A. E. Terabit free-space data transmission employing orbital angular momentum multiplexing. *Nat. Phot.* **2012**, *6*, 488−496.

(3) Su, Y.; He, Y.; Chen, H.; Li, X.; Li, G. Perspective on mode-division multiplexing. *Appl. Phys. Lett.* **2021**, *118*, 200502.

(4) Xu, H.; Dai, D.; Shi, Y. Silicon integrated nanophotonic devices for on-chip multi-mode interconnects. *Appl. Sci.* **2020**, *10*, 6365.

(5) Sit, A.; Bouchard, F.; Fickler, R.; Gagnon-Bischoff, J.; Larocque, H.; Heshami, K.; Elser, D.; Peuntinger, C.; Günthner, K.; Heim, B.; et al. High-dimensional intracity quantum cryptography with structured photons. *Optica* **2017**, *4*, 1006−1010.

(6) Krenn, M.; Handsteiner, J.; Fink, M.; Fickler, R.; Zeilinger, A. Twisted photon entanglement through turbulent air across Vienna. *Proc. Natl. Acad. Sci. U.S.A.* **2015**, *112*, 14197−14201.

(7) Fontaine, N. K.; Ryf, R.; Chen, H.; Neilson, D. T.; Kim, K.; Carpenter, J. Laguerre-Gaussian mode sorter. *Nat. Commun.* **2019**, *10*, 1865.

(8) Lightman, S.; Hurvitz, G.; Gvishi, R.; Arie, A. Miniature wide-spectrum mode sorter for vortex beams produced by 3D laser printing. *Optica* **2017**, *4*, 605−610.

(9) Berkhout, G.; Lavery, M.; Courtial, J.; Beijersbergen, M.; Padgett, M. J. Efficient sorting of orbital angular momentum states of light. *Phys. Rev. Lett.* **2010**, *105*, 153601.

(10) Piggott, A. Y.; Petykiewicz, J.; Su, L.; Vučković, J. Fabrication-constrained nanophotonic inverse design. *Sci. Rep.* **2017**, *7*, 1786.

(11) Wang, K.; Ren, X.; Chang, W.; Lu, L.; Liu, D.; Zhang, M. Inverse design of digital nanophotonic devices using the adjoint method. *Photonics Research,* **2020**, *8*, 528−533.

(12) Stern, B.; Zhu, X.; Chen, C. P.; Tzuang, L. D.; Cardenas, J.; Bergman, K.; Lipson, M. On-chip mode-division multiplexing switch. *Optica,* **2015**, *2*, 530−535.

(13) Frellsen, L. F.; Ding, Y.; Sigmund, O.; Frandsen, L. H. Topology optimized mode multiplexing in silicon-on-insulator photonic wire waveguides. *Opt. Express* **2016**, *24*, 16866−16873.

(14) Bozinovic, N.; Yue, Y.; Ren, Y.; Tur, M.; Kristensen, P.; Huang, H.; Willner, A. E.; Ramachandran, S. Terabit-scale orbital angular momentum mode division multiplexing in fibers. *Science* **2013**, *340*, 1545−1548.

(15) Sun, C.; Wade, M. T.; Lee, Y.; Orcutt, J. S.; Alloatti, L.; Georgas, M. S.; Waterman, A. S.; Shainline, J. M.; Avizienis, R. R.; Lin, S.; et al. Single-chip microprocessor that communicates directly using light. *Nature* **2015**, *528*, 534−538.

(16) Ye, J.; Li, Y.; Qu, S. On-Chip Orbital Angular Momentum Sorting with a Surface Plasmon Polariton Lens. *J. Light. Technol.* **2021**, *39*, 1423−1428.

(17) Ebbesen, T. W.; Genet, C.; Bozhevolnyi, S. I. Surface plasmon circuitry Phys. *Today* **2008**, *61*, 44.

(18) Sorger, V. J.; Oulton, R. F.; Ma, R.-M.; Zhang, X. Toward integrated plasmonic circuits. *MRS Bull.* **2012**, *37*, 728−738.

(19) Epstein, I.; Lilach, Y.; Arie, A. Shaping plasmonic light beams with near-field plasmonic holograms. *JOSA B* **2014**, *31*, 1642−1647.

(20) Zhang, P.; Wang, S.; Liu, Y.; Yin, X.; Lu, C.; Chen, Z.; Zhang, X. Plasmonic Airy beams with dynamically controlled trajectories. *Opt. lett.* **2011**, *36*, 3191−3193.

(21) Tsur, Y.; Epstein, I.; Remez, R.; Arie, A. Wavefront shaping of plasmonic beams by selective coupling. *ACS Photonics,* **2017**, *4*, 1339−1343.

(22) Fisher, C.; Botten, L. C.; Poulton, C. G.; McPhedran, R. C.; de Sterke, C. M. Efficient end-fire coupling of surface plasmons in a metal waveguide. *JOSA B* **2015**, *32*, 412−425.

(23) Olsthoorn, M.; Panichella, A. Multi-objective Test Case Selection Through Linkage Learning-Based Crossover. In *Search-Based Software Engineering: Proceedings of the 13th International*

Symposium (SSBSE 2021); O'Reilly, U.-M., Devroey, X., Eds.; Springer, 2021. DOI: 10.1007/978-3-030-88106-1_7.
(24) Thierens, D. The Linkage Tree Genetic Algorithm. *Lect. Notes Comput. Sci.* **2010**, *6238*, 264−273.
(25) Di Domenico, G.; Weisman, D.; Panichella, A.; Roitman, D.; Arie, A. *Planar on-Chip Mode Sorter*. DOI: 10.5281/zenodo.5115118 (accessed 2021-12-16).
(26) Johnson, P. B.; Christy, R. W. Optical constants of the noble metals. *Phys. Rev. B* **1972**, *6*, 4370.
(27) Koch, U.; et al. A monolithic bipolar CMOS electronic−plasmonic high-speed transmitter. *Nat. Electron.* **2020**, *3*, 338−345.
(28) Weisman, D.; Arie, A. Dynamic control of plasmonic beams. *Opt. Lett.* **2019**, *44*, 3689−3692.

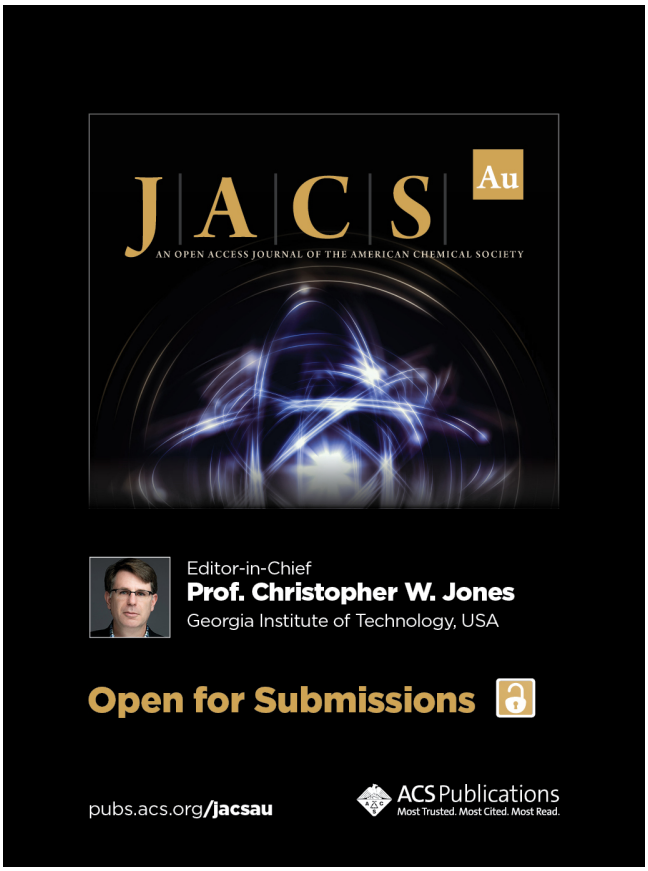

https://doi.org/10.1021/acsphotonics.1c01539
ACS Photonics 2022, 9, 378−382